



Highly-selective MOF-303 membrane for alcohol dehydration

Jun-Yu Lai ^a, Ting-Yuan Wang ^a, Changlong Zou ^b, Jiun-Jen Chen ^{c,***}, Li-Chiang Lin ^{a,b,**},
Dun-Yen Kang ^{a,*}

^a Department of Chemical Engineering, National Taiwan University, No. 1, Sec. 4, Roosevelt Road, Taipei, 10617, Taiwan

^b William G. Lowrie Department of Chemical and Biomolecular Engineering, The Ohio State University, 151 W. Woodruff Avenue, Columbus, OH, 43210, United States

^c Green Energy and Environment Research Laboratories, Industrial Technology Research Institute, No. 195, Sec. 4, Chung Hsing Road, Hsinchu, 31040, Taiwan



ARTICLE INFO

Keywords:

Metal-organic framework
MOF membrane
Pervaporation
Alcohol dehydration

ABSTRACT

Metal-organic frameworks (MOFs) are an emerging class of crystalline microporous materials, which have drawn considerable attention for separation applications. While a number of successful examples of MOF-based membranes for gas separation have been reported, only a few of pure MOF membranes presented high performance in pervaporation. This work reports on the application of a highly hydrophilic MOF, MOF-303, for dehydration of ethanol as well as isopropanol (IPA) via pervaporation. Dense MOF-303 membranes are fabricated with either a sodium hydroxide or urea solution. The latter recipe renders MOF-303 crystals a low quantity of missing linker; and it also yields a membrane with fewer pinhole-type defects. The MOF-303 membrane prepared with urea presents a relatively low air permeance and much higher separation performance for of water-ethanol and water-IPA mixtures, as compared to that synthesized with sodium hydroxide. The MOF-303-urea membrane possesses high separation factors for water/ethanol (55349) and for water/IPA (3801) at 303 K. At a higher temperature of 343 K, this membrane still offers a good water/ethanol separation factor of 1874. A 7-day pervaporation operation on the MOF-303-urea membrane demonstrates that the separation performance drops gradually during the test, but it can be restored via a thermal treatment on the membrane. Molecular simulations are performed to shed light on the transport property of water, ethanol, and IPA in MOF-303. The computational results suggest that the dehydration capability of this MOF can be attributed to both of its water-selective adsorption and diffusion, particularly the latter. Specifically, a relatively high diffusion barrier to the alcohols in MOF-303 results in the high selectivity of water over ethanol or IPA.

1. Introduction

Ethanol and isopropanol (IPA) serve as important energy resources and solvents [1–3]. Their purification typically involves thermodynamically driven processes, e.g., distillation, that are associated with high energy consumption [4–8]. Pervaporation is a membrane-based separation technique, which is considered as an energy-efficient alternative for alcohol purification [9–15]. In the past decades, polymeric membranes have been widely studied for the applications of alcohol dehydration via pervaporation. Various kinds of polymers have been demonstrated to offer good pervaporation performance, including poly(vinyl alcohol) [16–19], chitosan [20–23], polysulfone [24–27], polyimide [28–31], and polyamide [32–35]. Besides, poly(ionic liquid) has

also been investigated in recent years as a new class of materials for pervaporation [36,37]. Some of the polymeric materials have been further processed in a form of hollow fiber membranes [35,38–41], which are considered scalable for the industrial applications. While a number of polymeric membranes have been demonstrated to possess high separation performance for pervaporation, it remains challenging for these materials to achieve long-term stability under harsh operation conditions.

Inorganic ultramicroporous (pore size <0.7 nm [42]) materials are considered emerging materials for membrane pervaporation, aiming for robust operation under harsh conditions. Polycrystalline zeolite films, typically grown on porous ceramic substrates, have emerged as a good candidate for pervaporation. The highly-ordered channels with tunable

* Corresponding author. Department of Chemical Engineering, National Taiwan University, No. 1, Sec. 4, Roosevelt Road, Taipei, 10617, Taiwan.

** Corresponding author. Department of Chemical Engineering, National Taiwan University, No. 1, Sec. 4, Roosevelt Road, Taipei, 10617, Taiwan.

*** Corresponding author. Green Energy and Environment Research Laboratories, Industrial Technology Research Institute, No. 195, Sec. 4, Chung Hsing Road, Hsinchu, 31040, Taiwan.

E-mail addresses: JiunJenChen@itri.org.tw (J.-J. Chen), lclin@ntu.edu.tw (L.-C. Lin), dunyen@ntu.edu.tw (D.-Y. Kang).

hydrophilicity offers zeolite membranes high separation performance for water-alcohol mixtures. Several types of zeolite membranes have been made commercially available. For instances, the commercially available zeolite CHA membranes were reported to offer a high water/ethanol separation factor of over 60000 with a total flux of $0.9 \text{ kg m}^{-2} \text{ h}^{-1}$ [43]. Zeolite LTA membranes have also been commercialized, and they possessed a water/ethanol separation factor of over 10000 and a total flux of $3.5 \text{ kg m}^{-2} \text{ h}^{-1}$ [44]. Amorphous organosilica membranes were also demonstrated to offer excellent pervaporation performance for the water/alcohol separations [45–48]. In recent years, several emerging classes of inorganic materials, such as MXene [23,49,50] and graphene oxide [16,51,52], were blended with polymers to make mixed matrix membranes for alcohol dehydration.

Metal-organic frameworks (MOFs), aside from the aforementioned inorganic materials, offer new opportunities for membrane pervaporation. A MOF structure is formed by coordination of organic linkers to metal clusters, which enables a delicate control of pore size as well as surface functionality. In the past decade, a number of highly performing MOFs have been applied to catalysis [53–56], adsorption [57–60], and membrane gas separation [61–64]. However, the development of pure MOF membranes for pervaporation was relatively slow, likely owing to the stability issue of MOFs being in contact with water-alcohol mixtures. UiO-66 membranes were successfully fabricated on hollow fibers, which possessed a high stability under harsh environments and offered a high water/isobutanol separation factor (over 45000) and total flux ($4.81 \text{ kg m}^{-2} \text{ h}^{-1}$) [65]. ZIF-71 membranes were fabricated by the contra-diffusion method on an $\alpha\text{-Al}_2\text{O}_3$ tubular substrate. However, it had a relatively poor ethanol/water separation factor of 6.88 [66]. The CAU-10-H membranes were capable of being operated in acidic solutions, and offered a water/ethanol separation factor of 324 and a total flux of $0.397 \text{ kg m}^{-2} \text{ h}^{-1}$ [67]. The rare-earth MOF membranes, Sm-DOBDC, displayed high performances among pure MOF membranes. The water/ethanol separation factor was as large as 997 and total flux was $0.58 \text{ kg m}^{-2} \text{ h}^{-1}$ [68]. A pillared-bilayer MOF, Zn-aip-azpy, was as well made into a membrane form for the separation of water/IPA [69]. The separation factor of water/IPA for Zn-aip-azpy membranes achieved over 400, but the flux was relatively low ($0.077 \text{ kg m}^{-2} \text{ h}^{-1}$).

Hydrophilic MOFs can be potentially used for membrane pervaporation. Recently, MOF-303 with a pore limiting diameter of 5.84 \AA (Fig. 1) was reported to possess a high water uptake (up to $500 \text{ cm}^3 \text{ g}^{-1}$ at 303 K) [70]. The MOF-303 membranes grown on an $\alpha\text{-Al}_2\text{O}_3$ substrate have been applied in reverse osmosis [71]. The membranes displayed a high rejection rate of divalent ions (94% for MgCl_2 and 96% for Na_2SO_4) and a high water permeability ($3.0 \text{ L m}^{-2} \text{ h}^{-1} \text{ bar}^{-1} \mu\text{m}$). In this study, we report on the applications of MOF-303 membranes for the pervaporation with water/ethanol as well as water/IPA. Two recipes were proposed for the synthesis of MOF-303, in order to control the number of missing linkers within the MOF crystals as well as the intercrystalline defects within the membranes. 7-day pervaporation tests were performed for assessing the robustness of the MOF-303 membranes. X-ray diffraction (XRD) with synchrotron radiation source was used for investigating the structural change of MOF-303 following an exposure to the alcohols. Temperature-dependent experiments as well as pure-fluid pervaporation tests were conducted to gain insight into the mass transport in the membranes. State-of-the-art molecular simulations were also employed to shed light on the adsorption and diffusion properties of water/alcohols in MOF-303.

2. Experimental methods

2.1. Chemicals and materials

The chemicals used in this work included aluminum chloride hexahydrate ($\text{AlCl}_3 \cdot 6\text{H}_2\text{O}$, 99%, Sigma-Aldrich), 3,5-pyrazoledicarboxylic acid monohydrate ($\text{H}_3\text{PDC-H}_2\text{O}$, 97%, Acros Organics), sodium hydroxide (NaOH , 98%, Fluka), urea (CON_2H_4 , J.T.Baker), ethanol (EtOH ,

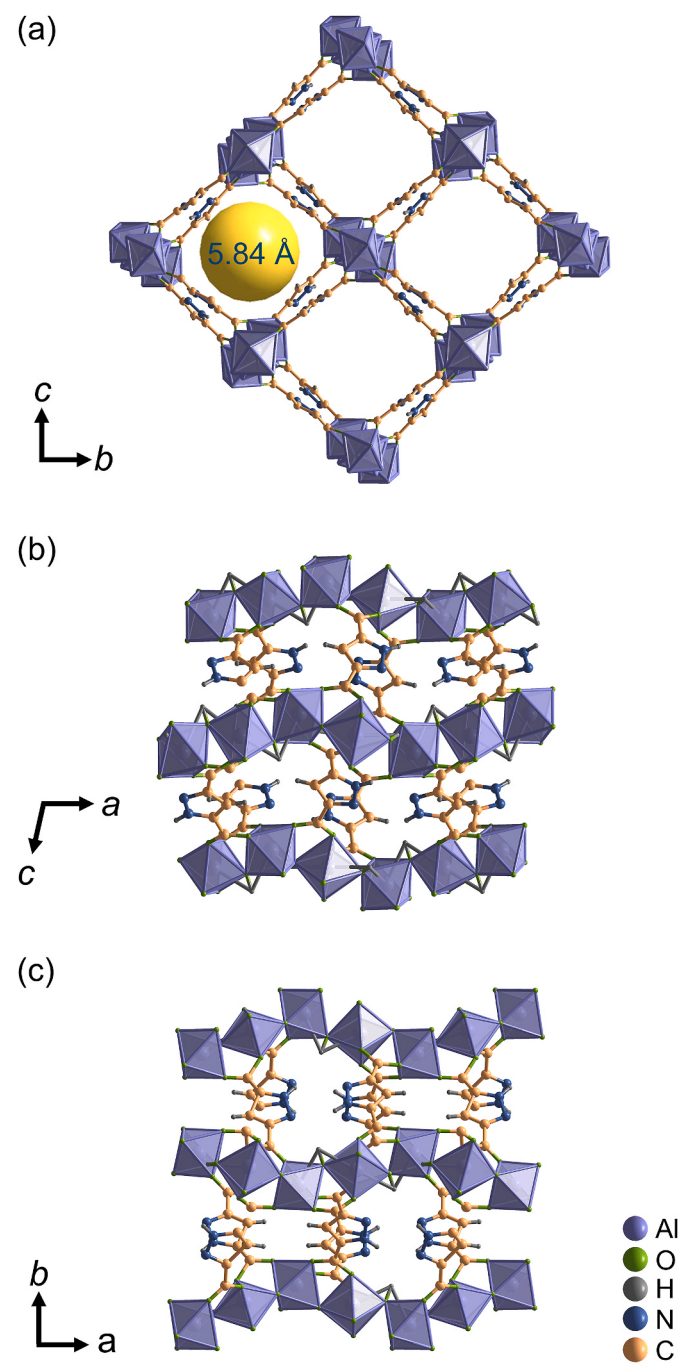


Fig. 1. Illustration of MOF-303 structure with views along the crystallographic (a) a -, (b) b -, and (c) c -axis.

$\geq 99.8\%$, Honeywell), and isopropanol (IPA, $\geq 99.8\%$, Honeywell). All reagents were used without further purification. The deionized water (DI water) was obtained from the ELGA VEOLIA PURELAB® ultrapure water system. The porous α -alumina disks were purchased from the Chao Yue Diamonds Limited Company (diameter = 40 mm and thickness = 2 mm), comprising α -alumina particles with an average particle size of approximately 300 nm and a porosity of 34%. The air permeance of the bare substrate is approximately $1.6 \times 10^{-6} \text{ mol m}^{-2} \text{ s}^{-1} \cdot \text{Pa}^{-1}$.

2.2. Synthesis of MOF-303 powder

MOF-303 in powder form was synthesized in accordance with the previously reported method [72] with minor modifications to create two

recipes, one with NaOH and the other with urea. For the synthesis of MOF-303 with NaOH, a solution comprising 2.6 g of NaOH in 30 g of DI water was first prepared. A separate solution was made with 0.578 g of AlCl₃·6H₂O and 0.417 g of H₃PDC·H₂O dissolved in 40 mL of DI water. This solution was mixed with 2.083 mL of the NaOH solution. The mixture was heated at 100 °C for 24 h under agitation. Following the reaction, the white powder was collected via vacuum filtration, during which the product was rinsed with DI water. The powder, referred to as MOF-303-NaOH powder, was dried at 100 °C overnight prior to use. For the recipe with urea, a solution comprising 3.9 g of urea in 30 g of DI water was first prepared. A separate solution with 0.722 g of AlCl₃·6H₂O and 0.521 g of H₃PDC·H₂O dissolved in 100 mL of DI water was made. This solution was mixed with 2.65 mL of the urea solution. The mixture was heated at 110 °C for 16 h under agitation. The MOF-303-urea powder was collected via vacuum filtration and then dried at 100 °C overnight.

2.3. Synthesis of MOF-303 membranes

MOF-303 membranes were prepared by the seeded growth method [61–63]. A suspension was prepared by adding 0.050 g MOF powder (MOF-303-NaOH or MOF-303-urea) in 10 g of DI water. The suspension was sonicated for 1 h prior to the spin-on deposition. Approximately 3 mL of suspension was dropped on an α-alumina substrate for the spin-on deposition, which was conducted at 3000 rpm for 30 s using a Laurell spin-coater (Model-WS-650MZ-23NPPB). The sample was then dried at 100 °C overnight before the secondary growth, which is described below.

The α-alumina substrate with a seed layer, being fixed in a Teflon holder, was placed in a 500-mL flask (Fig. S1), where the seed layer faced the bottom of the flask. The solution for the secondary growth of MOF-303 membrane was added into the flask, and then refluxed at 110 °C for 16 h. This solution consisted of AlCl₃·6H₂O (0.722g), H₃PDC·H₂O (0.521 g), DI water (100 mL), and a basic solution (2.65 mL). The basic solution was prepared by either of the two recipes: NaOH (2.6 g) in DI water (30 g) or urea (3.9 g) in DI water (30 g). The membrane following the secondary growth was rinsed with DI water to remove particulate on the membrane surface. It was then dried at 70 °C prior to use. The membrane prepared with NaOH was referred to as MOF-303-NaOH membrane, and that with urea was referred to as MOF-303-urea membrane hereafter.

2.4. Materials characterization

X-ray diffraction (XRD) was performed using a Rigaku SmartLab SE diffractometer with Cu Kα radiation at a wavelength of 1.5418 Å. The powder X-ray diffraction (PXRD) patterns were acquired from 5 to 40° 2θ with a step size of 0.02° 2θ. The scanning rate was set to be 8° 2θ per minute. The grazing-incidence X-ray diffraction (GIXRD) patterns for membranes were acquired from 5 to 40° 2θ with a step size of 0.02° 2θ. The scanning rate was set to be 5° 2θ per minute, and the incident angle of X-ray was set to be 0.5°.

The high-resolution XRD was performed in Taiwan Photon Source (TPS) 19A station at the National Synchrotron Radiation Research Center (NSRRC). The wavelength of the synchrotron X-ray source was 0.77489 Å. Approximately 1 mg of the powder sample was placed in a capillary tube, followed by an injection of 10 μL of ethanol or IPA into the tube. The MOF powder samples were treated with either ethanol or IPA for 6 days prior to the XRD analysis. The XRD patterns were recorded by a MYTHEN 18K position-sensitive detector under an exposure time of 3 s.

The morphology of the powder and membranes was characterized using a JEOL JSM-7600F field emission scanning electron microscope (FE-SEM) operated at an acceleration voltage of 10 kV. Prior to imaging, the samples were coated with platinum through sputtering deposition at a current of 10 mA for 90 s.

Thermogravimetric analysis (TGA) was performed on a TA Instruments SDT 650. The powder sample was subject to a heating program from 30 to 850 °C at an elevation rate of 10 °C per min. The measurements were conducted under an air flow at 100 mL per min.

The water vapor adsorption was conducted using a homemade setup. Approximately 0.7 g of MOF powder was used for the measurement. The sample was outgassed at 80 °C for 1 h prior to the measurement. The adsorption isotherm was obtained from 20 to 90% of relative humidity at 30 °C.

2.5. Pervaporation

The membrane pervaporation tests were performed using a homemade setup (Fig. S2). A membrane sample was placed in a stainless steel holder sealed with an o-ring. One side of the membrane was in contact with the feed solution composed of 90 wt% of ethanol or IPA in water. During the operation, the permeate side of the membrane was subjected to a reduced pressure of approximately 0.01 torr, and the feed solution was kept at a constant temperature (303, 313, 323, 333, or 343 K) under agitation. A typical operation lasted 3 h, including 1 h for the vapor-liquid equilibrium followed by 2 h for harvesting the vapor on the permeate side. The vapor was collected using a cold trap cooled with liquid nitrogen. The mass flux through the tested membrane was calculated using the following equation:

$$J = \frac{W}{A \cdot t} \quad (1)$$

where J is total mass flux, W is weight of the water-alcohol mixture collected on the permeate side, A is effective membrane area allowing for mass transport, and t is duration of the operation. The concentration of the water-alcohol mixture acquired on the permeate side was quantified using gas chromatography (GC). A SHIMADZU GC-2014 with a TCD detector was used for the analysis. The separation factor was quantified as the ratio of the weight fraction of alcohol (ethanol or IPA) on the permeate side to that on the feed side.

The permeability of water, ethanol, or IPA was computed using the following equation:

$$P_i = \frac{j_i \cdot h}{\gamma_i \cdot x_i \cdot P_i^{sat} - P_p} \quad (2)$$

where P_i and j_i are respectively permeability and molar flux of species i ; x_i , γ_i , and P_i^{sat} are respectively molar fraction, activity coefficient, and saturation vapor pressure of species i on the feed side; P_p is pressure on the permeate side, which is assumed to be zero; h is membrane thickness, which is assumed to be 2 μm based on the SEM characterization. The activity coefficients were computed using the modified UNIFAC model (see Table S1 for details). The permeation selectivity between two species in a mixture was computed as the ratio of the permeability of the two components. The values of molar flux for a species measured at various temperatures were used for deriving the activation energy for permeation of the species:

$$j_i = j_{i,0} \cdot \exp\left(\frac{-E_{a,i}}{R \cdot T}\right) \quad (3)$$

where $j_{i,0}$ is the pre-exponential factor, $E_{a,i}$ is the activation energy, R is the gas constant, and T is temperature.

2.6. Air permeation

The air permeation tests were performed using a homemade setup (Fig. S3). The membrane was sealed with aluminum foil tape and epoxy to prevent the leakage of air. Prior to a measurement, the downstream of the membrane was vacuumed for 4 h, while the upstream of the membrane was exposed to ambient air. The downstream was then disconnected from the vacuum pump, and its pressure started to increase due

to transmembrane air permeation from the upstream. The increase of the downstream pressure was monitored via a pressure gauge (ULVAC GP-1000). The air permeation flux was calculated using the following equation:

$$N = \frac{V}{A \cdot R \cdot T} \left(\frac{dP}{dt} \right) \quad (4)$$

where N is molar flux of air permeating through the membrane, $(\frac{dP}{dt})$ is the rate of pressure increase at the downstream, V is the downstream volume (0.3 L), A is effective area of membrane, R is the gas constant, and T is temperature. The air permeance was calculated as the molar flux of air divided by the transmembrane pressure difference, which is assumed to be 1 atm.

2.7. Molecular simulations

The adsorption selectivity of water over ethanol or IPA in the bulk structure of MOF-303 at temperatures of 303 K and 333 K was computed using the isobaric-isothermal and Gibbs ensemble Monte Carlo (NPT-GEMC) technique as implemented in the open-source RASPA [73] code. Two simulation boxes were constructed; one contained the MOF-303 structure and the other one contained the alcohol and water mixture at an alcohol concentration of approximately 90 wt% and a pressure of 1 bar. Because of the adsorption of adsorbate molecules into the MOF structure, the liquid mixture concentration will deviate from the target concentration, particularly at the initial stage of the simulations. Therefore, during the NPT-GEMC simulations, the liquid box was replaced at a frequency of every 20,000 Monte Carlo steps with the fully equilibrated liquid mixture at the target concentration. This process continued until the number of adsorbed water and alcohol in the MOF structure remained approximately a constant. In these calculations, intermolecular adsorbate-adsorbate and adsorbent-adsorbate interactions were described using 12-6 Lenard-Jones (L-J) potential and Coulombic interactions with static point charges. The L-J potential was truncated and shifted to zero at a cutoff radius 12 Å, and the long-range electrostatic potential was computed using the Ewald technique. The OPLS-AA force field [74] and the TIP3P model [75] were used to describe the alcohol and water molecules, respectively, while the universal force field (UFF) [76] was adopted for MOFs. The Lorentz-Berthelot mixing rules was applied to estimate the L-J parameters of different atoms. The atomic charges for the MOF structure were assigned by using the so-called *m*-CBMC method [77] developed by Lin and co-workers. The *m*-CBAC method is a supervised machine learning model that was trained based on charges that were computed by density functional theory. It should be noted that the alcohol molecules in these Monte Carlo simulations were treated as rigid for simplicity and accelerated calculations. The framework was also assumed to be rigid with their atomic positions determined by employing the Rietveld refinement on the experimentally obtained XRD pattern in this study. Note also that, considering the recognized concerns of Monte Carlo techniques in simulating the formation of water clusters [78–80], the NPT-GEMC calculations that were conducted herein used “water-saturated” MOF-303 structures as the starting point. That is, in contrast to employing an empty framework, frameworks loaded with water were used.

Molecular dynamics (MD) simulations were conducted as implemented in the LAMMPS [81] package to compute the diffusivity of pure alcohol and water molecules in their saturated condition which was determined using the above-mentioned NPT-GEMC simulations. These calculations were carried out in a canonical ensemble (NVT) at 303K and 333K. The force field adopted in the MD calculations was the same as the above Monte Carlo simulations, except that the alcohols were treated as flexible molecules. Bond stretching, angle bending, dihedral torsion, and 1–4 van der Waals contribution were used to describe intramolecular interactions. The long-range electrostatic interactions were computed

using the particle-particle-particle-mesh (pppm) method. The timestep was set to 0.5 fs and simulation time was at least 40 ns. The collected molecular trajectories were used to calculate the mean squared displacement (MSD) with an in-house script. The diffusion coefficient was subsequently calculated using the Einstein’s equation.

The Helmholtz free energy profiles for alcohol and water molecules were computed in order to shed light on the diffusion coefficients calculated from the abovementioned MD simulations. The collected molecular trajectories from MD simulations were first projected onto the permeation direction, followed by the calculation of their concentration as a function of the location along the permeation channel. With the concentration profile, the free energy profile can be accordingly determined via

$$\Delta A = -k_b T \ln\left(\frac{C_i(x)}{C_{i, \text{ref}}}\right) \quad (5)$$

where k_b is the Boltzmann constant, T is the temperature, C_i is the water or alcohol concentration at a specific position x , and $C_{i, \text{ref}}$ is the reference concentration of water or alcohol. Here, the reference is chosen as the maximum concentration along the permeation channel.

3. Results and discussion

In this work, we synthesized MOF-303 powder or membrane with two recipes. The sample synthesized with a NaOH solution is referred to as MOF-303-NaOH, and that with a urea solution is referred to as MOF-303-urea. The SEM images, XRD patterns, and water adsorption isotherms of the two MOF-303 powder samples are summarized in Fig. 2. The morphology characterization by SEM suggests that these two samples possess distinct particle size. MOF-303-NaOH presents a uniform particle size in sub-micrometer region, and its crystal morphology appears to be more amorphous in comparison to MOF-303-urea, which has a larger particle size ranging from 1 to 3 μm. According to the XRD characterization, both powder samples show patterns that are highly similar to the simulated XRD pattern from the crystallographic information file (CCDC #2078717), indicating both of these MOFs possess a pure MOF-303 phase. The water adsorption isotherms obtained at 30 °C suggests that MOF-303 has a higher water uptake than CAU-10-H [67] or Zn-aip-apzy [69], both of which have been used for membrane pervaporation. The large water adsorption quantity suggest that MOF-303 could serve as a water-selective membrane. MOF-303-urea presents a slightly higher water adsorption uptake than MOF-303-NaOH at relative humidity below 80%, and this could be attributed to quantity of missing linkers in the crystals. TGA was used for quantifying the missing linkers (Fig. S4) [82]. MOF-303-urea is found to have a lower amount of missing linker (10%) than MOF-303-NaOH did (23%). The lower quantity of missing linkers for MOF-303-urea may render it a higher crystallinity and thus a higher water adsorption capacity [83]. Interestingly, the weight loss appearing in the TGA curves below 200 °C also suggests that MOF-303-urea adsorbs more water than MOF-303-NaOH under an ambient condition.

The MOF-303 membranes were prepared via the seeded growth methods [61–63]. The SEM images of the bare alumina substrate as well as the substrates following a seed layer deposition are shown in Fig. S5. MOF-303-NaOH form a more uniform seed layer than MOF-303-NaOH-urea, because of its sub-micrometer particle size. The two MOF-303 membranes following the secondary growth also present distinct morphology (Fig. 3a). Specifically, the MOF-303-urea membrane possesses larger grains than the MOF-303-NaOH membrane does. Nevertheless, both membranes have a thickness of around 2 μm. According to the top- and side-view SEM images, micrometer-scale defects are absent in both samples. The GIXRD patterns of the two samples suggest that they both possess a pure phase of MOF-303 (Fig. 3b). Air permeation tests were performed to assess the pinhole-type defects in the MOF-303 membranes (Fig. S6). According to our previous report

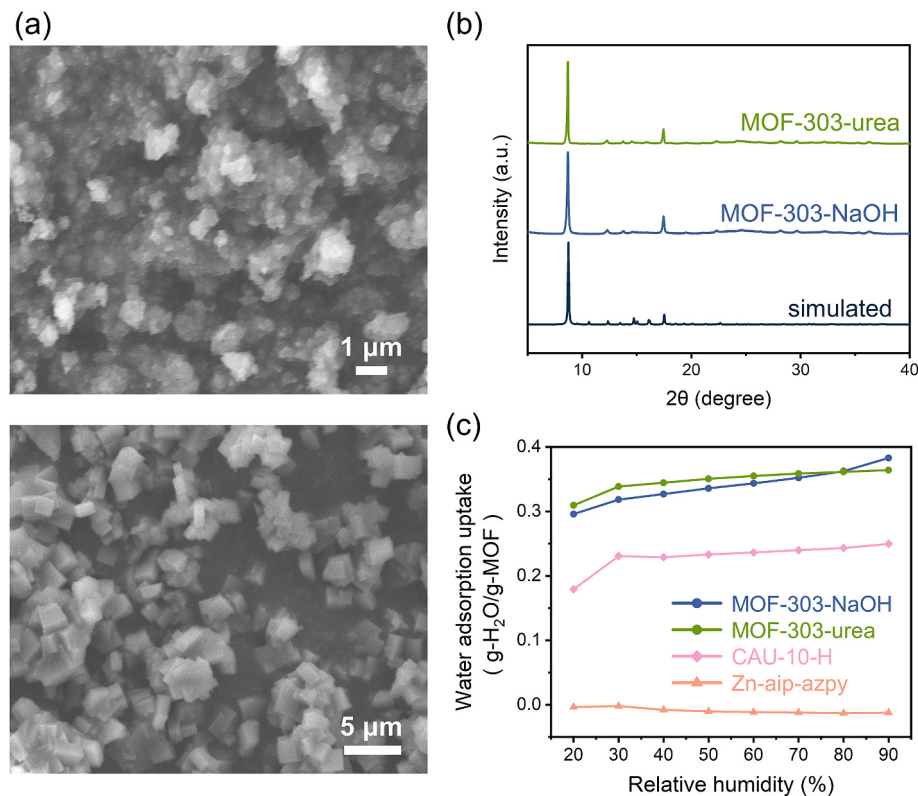


Fig. 2. (a) SEM images of MOF-303-NaOH (top) and MOF-303-urea (bottom) in powder form. (b) Powder XRD patterns and (c) water adsorption isotherms of MOF-303-NaOH and MOF-303-urea. The XRD patterns shown in (b) were obtained using an in-house facility with X-ray at a wavelength of 1.5418 Å. The isotherms from CAU-10-H and Zn-aip-azpy are included in (c) for comparison.

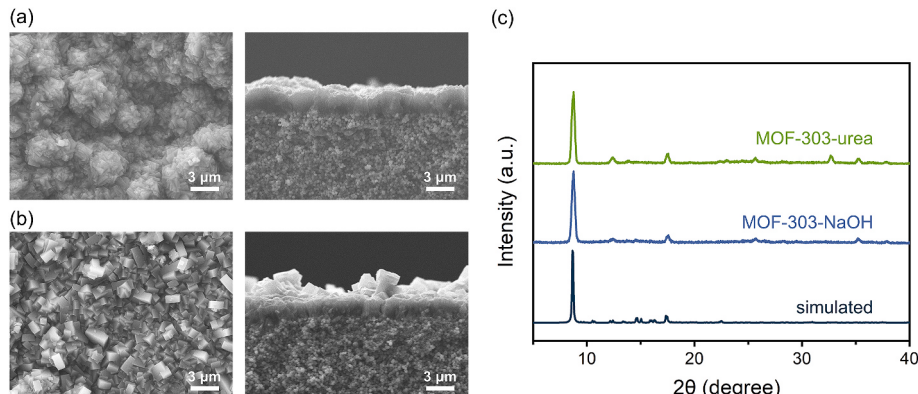


Fig. 3. Top- and side-view SEM images of (a) MOF-303-NaOH and (b) MOF-303-urea membrane. (c) XRD patterns of MOF-303-NaOH and MOF-303-urea membrane. The XRD patterns shown in (c) were obtained using an in-house facility with X-ray at a wavelength of 1.5418 Å.

[69], the air permeance of a membrane increases with the quantity of pinholes formed within. More importantly a membrane with air permeance beyond 10^{-8} mol m⁻² s⁻¹·Pa⁻¹ indicates that the pinhole-type defects are likely to dominate the mass transfer in the membrane. The MOF-303-NaOH sample possesses a high air permeance (7.9×10^{-8} mol m⁻² s⁻¹·Pa⁻¹), and it also presents a very low separation factor of water over IPA (5.46) at 30 °C. In contrast, the MOF-303-urea sample has a relatively low air permeance (1.7×10^{-9} mol m⁻² s⁻¹·Pa⁻¹) and a high separation factor of water over IPA (3801). The surface characterization suggests that MOF-303-urea has a lower water contact angle than MOF-303-NaOH does (Fig. S7), indicating the former sample possesses a more hydrophilic surface. As the MOF-303-urea membrane seems to be less defective and more hydrophilic, the following investigation will be focused on this sample.

The MOF-303-urea membrane was subject to a 7-day pervaporation test with a water-ethanol or a water-IPA mixture at 333 K (Fig. 4). During the 7-day operation with the two kinds of feed solutions, the total mass flux of the membrane presents marginal fluctuations in the range of 0.1–0.2 kg m⁻² h⁻¹. For the first day, the separation factor of water over ethanol is as high as 1364, and that of water over IPA is 212. The separation factor of water over ethanol gradually decreases to 57 on the sixth day. A similar ageing effect is observed for the pervaporation with water/IPA. The ageing effect could be attributed to the framework swelling of MOF-303, which will be discussed below. Interestingly, after reactivating the MOF-303-urea membrane via heating it at 70 °C for 20 h, the separation performance was restored for both mixtures. Specifically, the separation factor of water over ethanol goes up to 1928, and that of water over IPA improves to 465 on the seventh day.

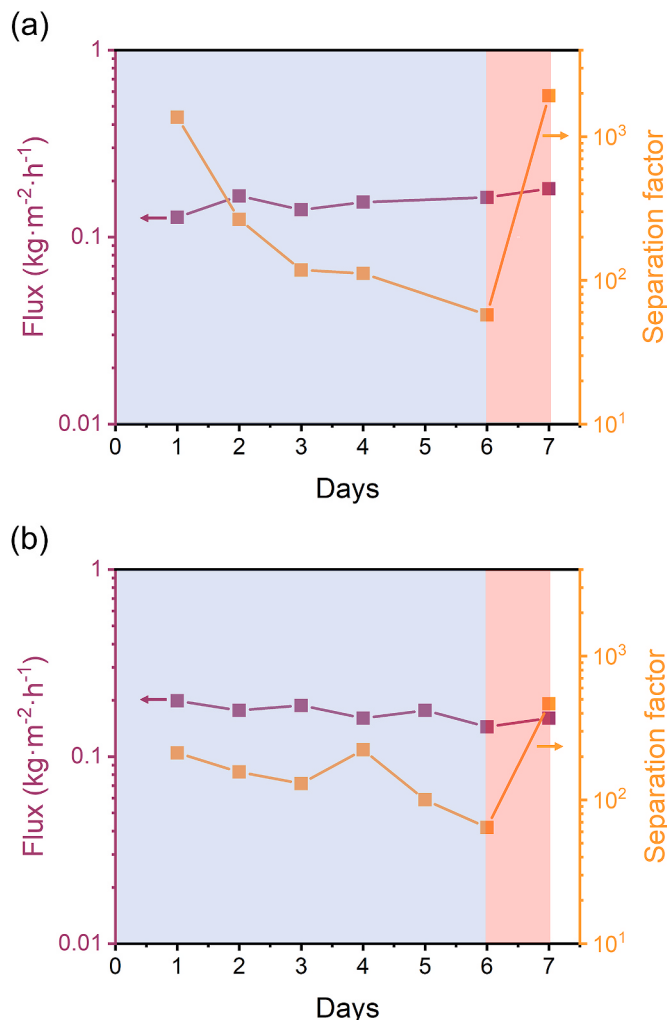


Fig. 4. Time-dependent flux and separation factor of the MOF-303-urea membrane subject to pervaporation tests with 90 wt% of (a) ethanol and (b) IPA at 333 K. On the sixth day, the membrane samples were reactivated via a thermal treatment at 70 °C for 20 h. The separation performance was found to be restored on the seventh day.

To investigate the possible swelling effect of MOF-303 initiated by alcohols, high-resolution XRD with a synchrotron X-ray source was performed on the MOF-303-urea powder sample, which was treated with ethanol or IPA before the analysis (Fig. S8). Following the treatment with alcohols, the (011) and (022) diffractions shift to lower angles, suggesting an enlarged lattice size of the MOF. The crystal structures of the treated MOF-303 were determined by the Rietveld refinement. The results suggest that the PLDs of the MOF-303-urea treated with ethanol and IPA for 6 days become 6.21 and 6.13 Å, respectively. These PLD values are considerably larger than that of the as-synthesized MOF-303-urea (5.84 Å), suggesting a swelling effect initiated by the alcohols. The swelling of the framework would significantly increase the permeability of ethanol or IPA, which could ultimately lower the water/alcohol selectivity. The XRD analysis shown in Fig. S9a suggests that the swelling effect is relieved following the thermal reactivation. The SEM images of the membrane samples (Fig. S9b-d) indicate that the crystal morphology of MOF-303 is not affected by being immersed in ethanol. In other words, the MOF-303 membrane is generally stable when being in contact with ethanol, despite a marginal enlargement in its crystal lattice.

Pervaporation tests with the MOF-303-urea membrane at various temperatures, ranging from 303 to 343 K, were performed (Fig. 5). For

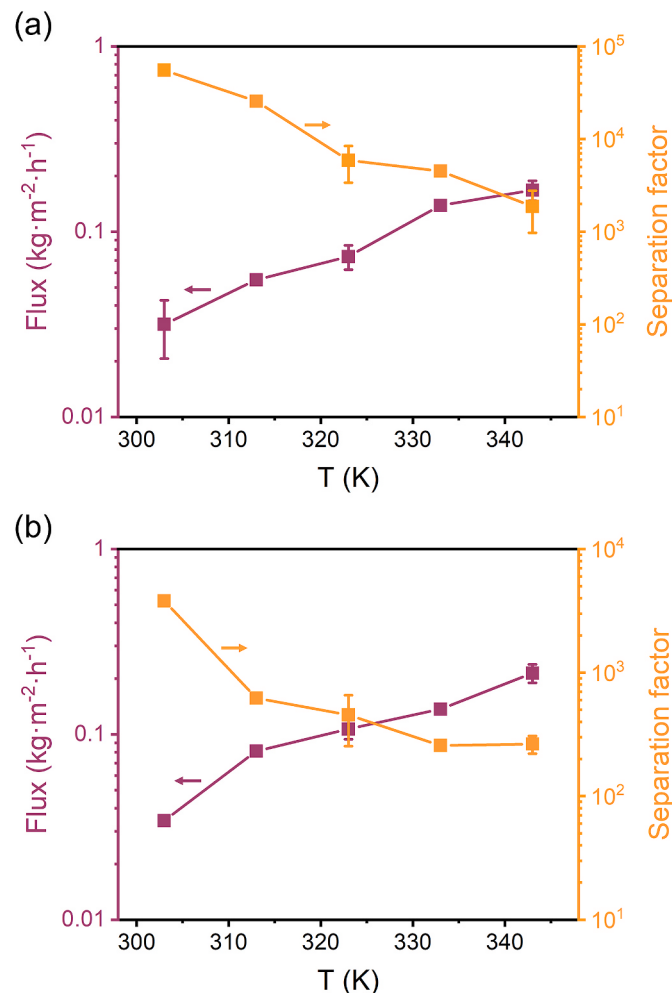


Fig. 5. Temperature-dependent flux and separation factor of the MOF-303-urea membrane subject to pervaporation tests with 90 wt% of (a) ethanol and (b) IPA.

the water-ethanol as well as water-IPA mixtures, the total mass flux increases with temperature, whereas the separation factor becomes lower at higher temperatures. At 303 K, the MOF-303 membrane possesses high separation factors of water over ethanol (55349) and water over IPA (3801). These two values, however, drop to 1874 and 264 at 343 K. We note that the separation factor is interestingly higher for water/ethanol than for water/IPA. As the kinetic diameter of IPA (4.7 Å) is larger than ethanol (4.3 Å), this finding is counterintuitive. This phenomenon will be addressed later with the molecular simulations. When the temperature increases from 303 to 343 K, the total flux is increased by 5 times for water/ethanol and 6 times for water/IPA. To gain insight into the molecular permeation in MOF-303, the Arrhenius equation (Eq. (3)) was applied to determine the activation energy for the permeation of water, ethanol, and IPA (Fig. S10). The activation energies for water permeation are 21.6 and 16.5 kJ/mol respectively for the water/ethanol and water-IPA mixture. The difference could be attributed to the higher driving force for the permeation of water in IPA, as the activity of water in the water-IPA mixture is higher than that in the water-ethanol mixture (Table S2). The larger driving force for water permeation might make the water flux less sensitive to the temperature change. The activation energies for ethanol and for IPA permeation are respectively 53.6 and 39.6 kJ/mol, both of which are considerably higher than that of water. This results in the high selectivity of water over ethanol for the MOF-303 membrane. The higher activation energy of ethanol than that of IPA also explains the higher separation factor of

water/ethanol than water/IPA.

The water/alcohol separation performance of MOF-303-urea and MOF-303-NaOH membranes are summarized in Fig. 6, along with the previously reported pure MOF and zeolite membranes [65,67–69,84–90]. The raw data are also tabulated in Table S2. The MOF-303-urea membrane possesses an extraordinarily high separation factor of water over ethanol, as compared to other pure MOF membranes. Its highest water/ethanol separation factor achieves 55349 for 90 wt% of ethanol at 303 K. While the separation factor gradually decreases with temperature, the MOF-303-urea membrane still presents outstanding separation performance for water/ethanol at 343 K (separation factor = 1874). For the separation of water/IPA, the MOF-303-urea membrane presents a high separation factor of 3801 at 303 K; and the value reduces to 264 at 343 K. While the flux of the MOF-303 membranes is not high enough compared to other MOF membranes, engineering approaches from different aspects could be applied to address this issue, such as creating structural defects (i.e., defect engineering), reducing the membrane thickness, or enhancing the convection in the feed reservoir to diminish concentration polarization.

We sought to shed light on the competitive effect for the transport of alcohols and water in MOF-303. Pervaporation tests with pure fluids (water, ethanol, or IPA) were conducted; and these results were compared to those with 90 wt% of alcohols as a feed at 333 K (Fig. 7). The permeabilities of the transport species were computed based upon the modified UNIFAC model, and the details for the calculation are summarized in Table S1. The water permeabilities are 4319, 1503, and 1198 Barrer from the tests with pure water, 90 wt% of ethanol, and 90 wt% of IPA, respectively. The results from the pervaporation operated with mixtures are the average values from the 7-day tests, which are shown in Fig. 4. The water permeabilities from the mixture pervaporation are lower than that from unary pervaporation, which may be attributed to the competitive effect of the binary-component diffusion. As for ethanol and IPA, we also observed lower permeabilities from the

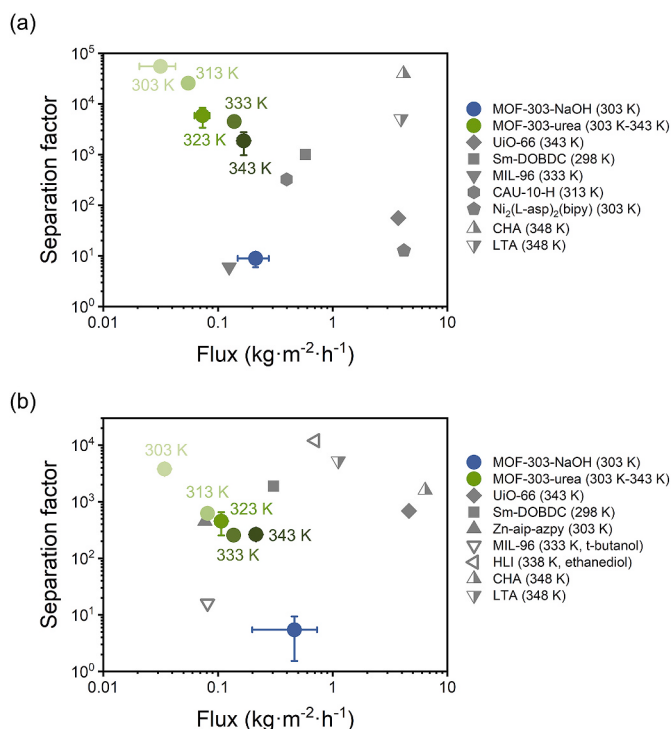


Fig. 6. Pervaporation performance of pure MOF membranes for (a) water/ethanol and for (b) water/IPA. The alcohol dehydration performance of zeolite CHA as well as LTA is also included for comparison. The dehydration performance of MOF membranes for other kinds of alcohols is also shown in (b). The raw data shown in this figure are tabulated in Table S2.

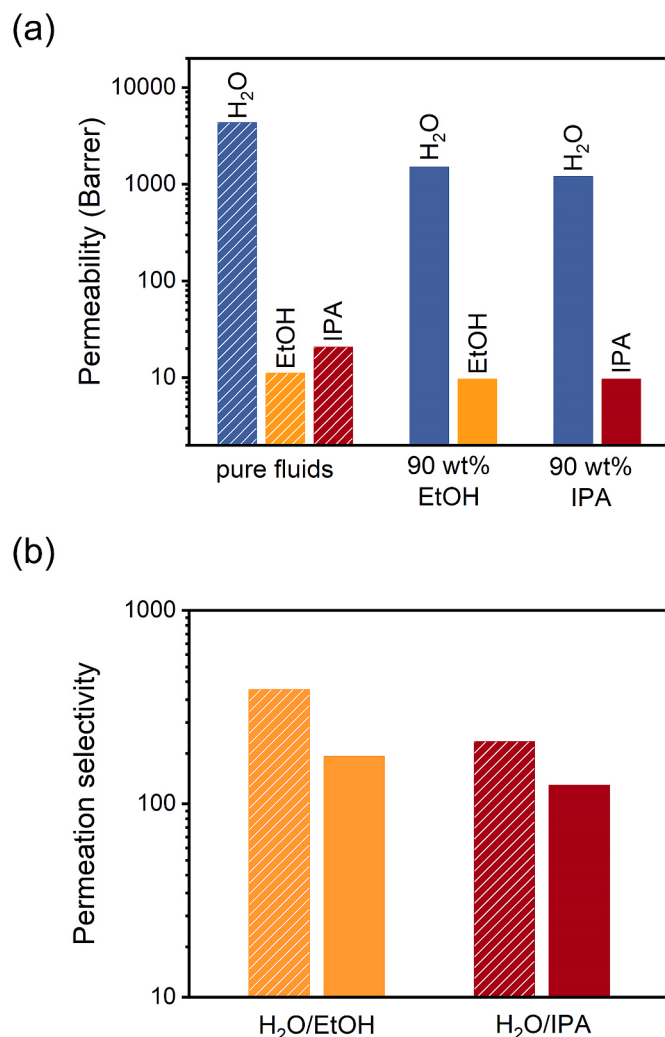


Fig. 7. (a) Permeabilities and (b) permeation selectivities from pervaporation tests with pure fluids (symbols with texture) and mixtures (filled symbols) for the MOF-303 membrane operated at 333 K. The mixtures used in these tests are 90 wt% of ethanol or IPA.

tests with mixtures as compared to those with pure fluids. The permeabilities of ethanol and IPA are respectively 11 and 21 Barrer from the pure-fluid tests, and these values drop to 9 and 10 from tests with mixtures. Interestingly, according to the pure-fluid measurements, the IPA permeability is almost twofold higher than the ethanol one, despite a larger kinetic diameter of IPA than ethanol (4.7 versus 4.3 Å). The micropore of MOF-303 seems to favor the diffusion of IPA than ethanol, and this results in a lower selectivity of water/IPA than water/ethanol. The ideal selectivities, obtained from the pure-fluid measurements, are 389 and 209 for water/ethanol and water/IPA, respectively. The selectivities of water/ethanol and water/IPA from the tests with mixtures are 176 and 124, respectively; and these values are nearly on par with the ideal selectivities.

Molecular simulations, specifically MD and NPT-GEMC calculations, were employed in order to achieve molecular-level understanding on the transport behavior of water and alcohols in MOF-303. The Helmholtz free energy profiles of the adsorbates deduced from MD trajectories are summarized in Fig. 8. A free energy profile represents the likelihood of an adsorbate molecule being present at a specific spot along the transport channel, from which a spot with a high free energy suggests a low probability of finding the adsorbate, and vice versa. The results suggest that the interior surface of MOF-303 is notably more homogeneous, in terms of free energy, to water than to alcohols. This can be partly

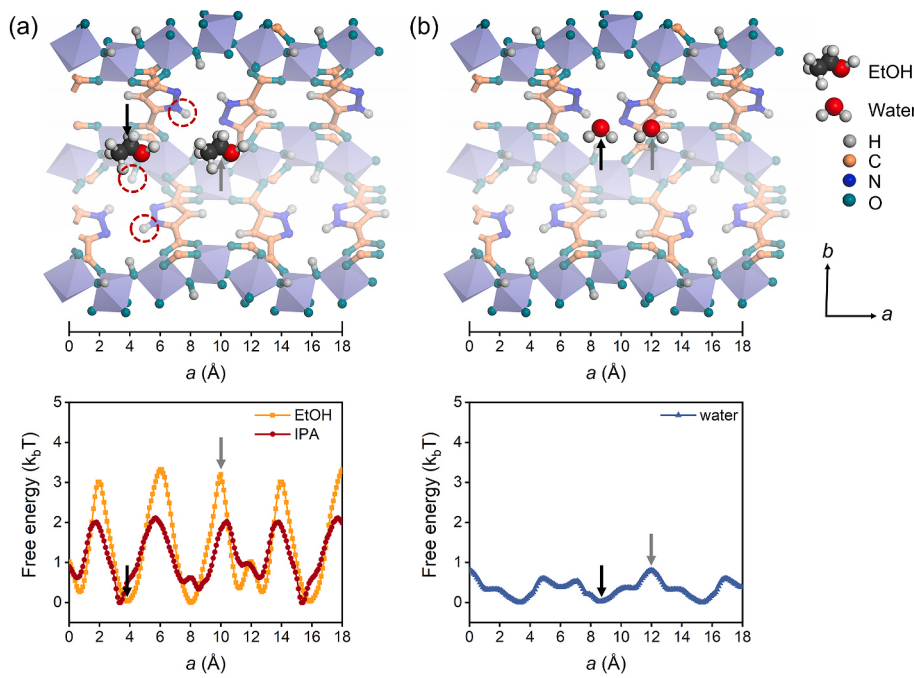


Fig. 8. (a) Illustration of ethanol in the channel of MOF-303 (top) and the corresponding Helmholtz free energy profiles of ethanol and IPA along the crystallographic a -axis (bottom). (b) Illustration of water in the channel of MOF-303 (top) and the corresponding Helmholtz free energy profile of water along the crystallographic a -axis (bottom). The dashed circles highlight the $-OH$ group from the metal cluster and the $-NH$ groups from the linker of MOF-303, which could form hydrogen bonds to an adsorbate. The black and gray arrows respectively indicate the local minimum and maximum locations of the free energy.

attributed to the hydrogen bonds formed between the adsorbate molecules and the linker of MOF-303, which has $-OH$ and $-NH$ groups. The adsorption sites for water in MOF-303 has been discussed in previous reports [83]. For an ethanol molecule locating at the spot of minimum free energy (around 4 Å at a -axis shown in Fig. 8a), the hydroxyl group of the adsorbate is in close proximity to multiple $-OH$ or $-NH$ groups from the framework. However, for the spot at which an ethanol molecule experiences a high free energy (around 10 Å at a -axis shown in Fig. 8a), its hydroxyl group is at a distance from an $-OH$ or an $-NH$ group of the MOF. The adsorbent-adsorbate interaction discussed above can also be applied to the transport of IPA in MOF-303. However, unlike ethanol or IPA, which has a hydrophobic group on one side and a hydrophilic group on the other side, a water molecule has hydroxyl groups on both ends. Such a nature renders water a relatively homogenous free energy profile along the channel of MOF-303. Specifically, as shown in Fig. 8b, wherever a water molecule is located, at least one hydroxyl group of water is in close proximity to an $-OH$ or $-NH$ group from the framework. This suggests that adsorbent-adsorbate interaction has low variation for a water molecule in the pore of MOF-303.

As the channel of MOF-303 is relatively homogeneous to water in terms of free energy, as compared to ethanol or IPA, a higher mean squared displace (MSD) was found for water from the MD simulations (Fig. S11). The higher MSD value of water suggests its higher diffusion coefficient than ethanol or IPA (Table S3). The effect of the energetic homogeneity of an adsorption surface on molecular diffusion had been discussed in our previous work for the transport of CO_2 in MOFs [91]. We note that the free energy barrier to ethanol was higher than that to IPA, which results in a lower diffusion coefficient of ethanol. As the adsorption uptake of ethanol is higher than that of IPA (Fig. S12 and Table S3), it might imply that the local adsorption sites in MOF-303 has a stronger interaction with ethanol than with IPA. This could ultimately lead the relatively high free energy barrier to ethanol. Nevertheless, the simulation results suggest that MOF-303 has a much higher water solubility than ethanol or IPA.

The computed adsorption selectivity from the NPT-GEMC simulations and the computed diffusion selectivity from MD simulations are summarized in Fig. 9. The computed adsorption selectivity for water/ethanol is 21, and that for water/IPA is 56. The high water/alcohol adsorption selectivity can be attributed the fact of two hydrophilic ends

(water) versus one (ethanol or IPA), as discussed above. IPA possesses a lower adsorption uptake than ethanol, likely due to its bulkier alkyl group that renders IPA a more hydrophobic nature than ethanol. The computed diffusion selectivity is 103 and 69 for water/ethanol and for water/IPA, respectively. The permeation selectivities, per the solution-diffusion model as the product of adsorption and diffusion selectivity, are 103 and 69 for water/ethanol and water/IPA, respectively. The computed permeation selectivity values are higher than those measured experimentally. Such a disagreement could be attributed to two facts. First, the diffusive selectivities obtained from simulations are computed with rigid frameworks (i.e., neglecting the effects of framework flexibility that a real MOF usually possesses). Such an assumption could lead to an overestimation of diffusive selectivity. Second, a trace amount of the pinhole-type defects could be present in the MOF-303 membrane, which would lower its separation performance.

4. Conclusions

We have demonstrated the application of MOF-303 membranes in dehydration of ethanol or IPA via pervaporation. We assessed the synthesis of dense MOF-303 membranes with urea or NaOH. The former recipe yields MOF crystals with a lower quantity of missing linkers, which results in a slightly higher water adsorption uptake. More importantly, the MOF-303-urea membrane presents a much lower air permeance than the MOF-303-NaOH one, suggesting a lower number of pinhole-type defects within the membrane. At 303 K, the MOF-303-urea membrane presents high separation factors of water over ethanol (55349) and water over IPA (3801). The separation factor for the MOF-303-NaOH membrane at 303 K is 9 and 5 for water/ethanol and water/IPA, respectively. During a 7-day pervaporation test with water/ethanol or water/IPA at 333 K, the separation factor of the MOF-303-urea membrane gradually reduces, while the total flux stays nearly unchanged. Interestingly, the separation performance of the membrane is found to be restored via a thermal reactivation. The high-resolution XRD analysis suggests that the PLD of MOF-303 increases from 5.84 Å to 6.21 and 6.13 Å after a 6-day exposure to ethanol and water, respectively. Temperature-dependent pervaporation experiments were conducted to obtained activation energy for the permeation of water, ethanol, and IPA, in MOF-303. The activation energy of ethanol or IPA is found to be

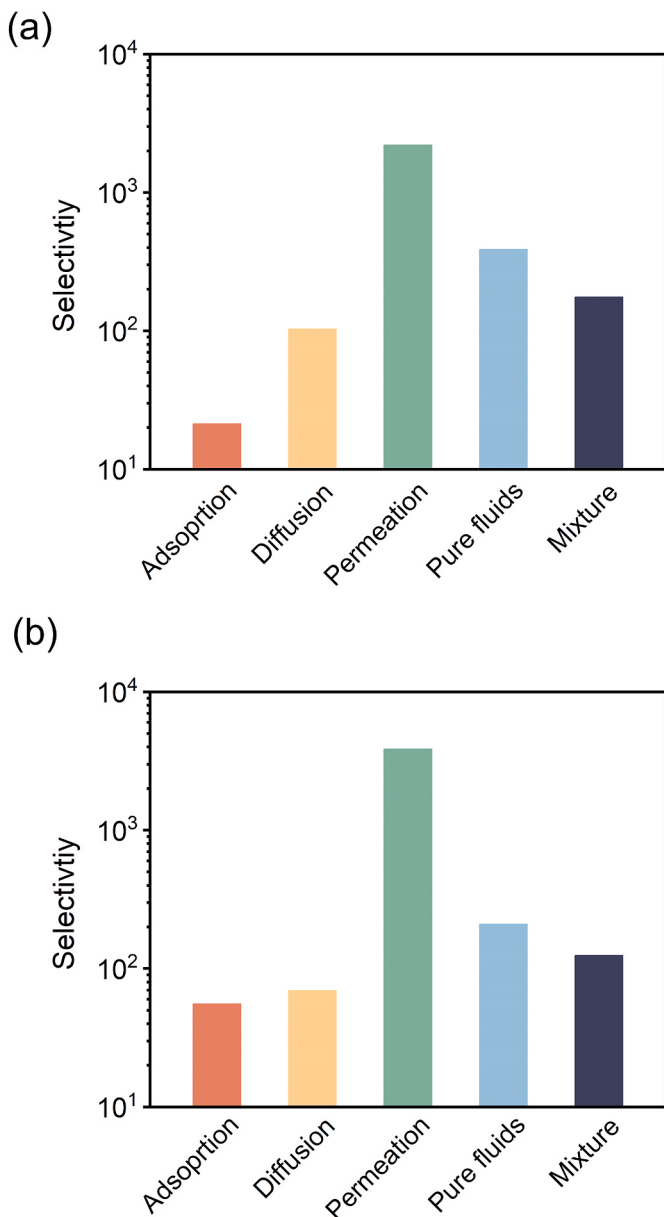


Fig. 9. Adsorption, diffusion, and permeation selectivities obtained from simulations as well as permeation selectivities obtained from experiments with pure fluids and mixtures for the separation of (a) water/ethanol and (b) water/IPA at 333 K.

higher than that of water, indicating that MOF-303 favors the transport of water than the alcohols. Molecular simulations were employed to understand the diffusion as well as adsorption behavior of water, ethanol, and IPA in this MOF. The computed free energy profile is much smoother for water than for ethanol or IPA. This can be partly attributed to the spatial arrangements of –NH and –OH groups on the surface of the MOF. Specifically, wherever a water molecule is located in the pore of MOF-303, at least one end of the water molecule is in a close proximity of an –OH or an –NH group. Such an energetically homogeneous surface to water renders MOF-303 a high water/alcohol selectivity. The results suggest the critical role of surface homogeneity, in terms of adsorbent-adsorbate interaction, in the design of new MOF membranes for molecular separations.

Author statement

Jun-Yu Lai: Investigation, Visualization, Writing – original draft, Writing – review & editing. Ting-Yuan Wang: Software, Visualization, Writing – original draft, Formal analysis. Changlong Zou: Software, Formal analysis. Jiun-Jen Chen: Resources, Writing – review & editing. Li-Chiang Lin: Conceptualization, Formal analysis, Writing – review & editing. Dun-Yen Kang: Conceptualization, Funding acquisition, Supervision, Project administration, Visualization, Writing – original draft, Writing – review & editing.

Declaration of competing interest

The authors declare that they have no known competing financial interests or personal relationships that could have appeared to influence the work reported in this paper.

Data availability

No data was used for the research described in the article.

Acknowledgments

This work was supported by the Bureau of Energy of the Ministry of Economic Affairs of Taiwan (Grant No.111-E0201). The authors would like to thank Su-Jen Ji and Chia-Ying Chien at the Instrumentation Center at National Taiwan University for their assistance in the SEM experiments using the JEOL JSM-7600F. We would also like to thank Yu-Chun Chuang and Chung-Kai Chang in TPS Beamline 19A at National Synchrotron Radiation Research Center (NSRRC) for the XRD measurements. The authors also thank the National Center for High-performance Computing (NCHC) in Taiwan for the computational resources.

Appendix A. Supplementary data

Supplementary data to this article can be found online at <https://doi.org/10.1016/j.memsci.2022.120879>.

References

- [1] W.-C. Chen, C.-T. Sheng, Y.-C. Liu, W.-J. Chen, W.-L. Huang, S.-H. Chang, W.-C. Chang, Optimizing the efficiency of anhydrous ethanol purification via regenerable molecular sieve, *Appl. Energy* 135 (2014) 483–489.
- [2] B. Mandal, S. Ghosh, S.P. Moulik, Interaction between a bio-tolerable amino-acid based amphiphile (N-dodecanoylsarcosinate, SDS) and modified cationic polymers, hydroxyethylcelluloses (JR 400, and LM 200) in isopropanol-water medium, *Colloids Surf. A Physicochem. Eng. Asp.* 566 (2019) 156–165.
- [3] F. Yasui, K. Sekiguchi, H. Tamura, Decomposition of 2-propanol in the liquid phase using a photocatalyst immobilized on nonwoven fabric and ozone microbubbles, *Water Air Soil Pollut.* 230 (11) (2019) 252.
- [4] C. Conde-Mejía, A. Jiménez-Gutiérrez, Analysis of ethanol dehydration using membrane separation processes, *Open Life Sci.* 15 (1) (2020) 122–132.
- [5] P.D. Chapman, T. Oliveira, A.G. Livingston, K. Li, Membranes for the dehydration of solvents by pervaporation, *J. Membr. Sci.* 318 (1) (2008) 5–37.
- [6] H. Li, C. Guo, H. Guo, C. Yu, X. Li, X. Gao, Methodology for design of vapor permeation membrane-assisted distillation processes for aqueous azeotrope dehydration, *J. Membr. Sci.* 579 (2019) 318–328.
- [7] S. Al-Obaidani, E. Curcio, F. Macedonio, G. Di Profio, H. Al-Hinai, E. Drioli, Potential of membrane distillation in seawater desalination: thermal efficiency, sensitivity study and cost estimation, *J. Membr. Sci.* 323 (1) (2008) 85–98.
- [8] E. Halakoo, X. Feng, Self-assembled membranes from polyethylenimine and graphene oxide for pervaporation dehydration of ethylene glycol, *J. Membr. Sci.* 616 (2020), 118583.
- [9] G. Liu, W. Jin, Pervaporation membrane materials: recent trends and perspectives, *J. Membr. Sci.* 636 (2021), 119557.
- [10] M. Wang, X. Cheng, G. Jiang, J. Xie, W. Cai, J. Li, Y. Wang, Preparation and pervaporation performance of PVA membrane with biomimetic modified silica nanoparticles as coating, *J. Membr. Sci.* 653 (2022), 120535.
- [11] B. Bolto, M. Hoang, Z. Xie, A review of membrane selection for the dehydration of aqueous ethanol by pervaporation, *Chem. Eng. Process: Process Intensif.* 50 (3) (2011) 227–235.

- [12] Y. Wu, L. Ding, Z. Lu, J. Deng, Y. Wei, Two-dimensional MXene membrane for ethanol dehydration, *J. Membr. Sci.* 590 (2019), 117300.
- [13] G. Yang, Z. Xie, A.W. Thornton, C.M. Doherty, M. Ding, H. Xu, M. Cran, D. Ng, S. Gray, Ultrathin poly (vinyl alcohol)/MXene nanofilm composite membrane with facile intrusion-free construction for pervaporation separations, *J. Membr. Sci.* 614 (2020), 118490.
- [14] C. Zou, L.-C. Lin, Exploring the potential and design of zeolite nanosheets as pervaporation membranes for ethanol extraction, *ChemComm* 54 (94) (2018) 13200–13203.
- [15] C. Zou, L.-C. Lin, Potential and design of zeolite nanosheets as pervaporation membranes for ethanol extraction, *Ind. Eng. Chem. Res.* 59 (28) (2020) 12845–12854.
- [16] R. Castro-Muñoz, J. Buera-González, Ó.d.l. Iglesia, F. Galiano, V. Fila, M. Malankowska, C. Rubio, A. Figoli, C. Téllez, J. Coronas, Towards the dehydration of ethanol using pervaporation cross-linked poly(vinyl alcohol)/graphene oxide membranes, *J. Membr. Sci.* 582 (2019) 423–434.
- [17] M.E. Dmitrenko, A.V. Penkova, A.I. Kuzminova, M. Morshed, M.I. Larionov, H. Alem, A.A. Zolotarev, S.S. Ermakov, D. Roizard, Investigation of new modification strategies for PVA membranes to improve their dehydration properties by pervaporation, *Appl. Surf. Sci.* 450 (2018) 527–537.
- [18] L. Liu, S.E. Kentish, Pervaporation performance of crosslinked PVA membranes in the vicinity of the glass transition temperature, *J. Membr. Sci.* 553 (2018) 63–69.
- [19] Q.G. Zhang, Q.L. Liu, A.M. Zhu, Y. Xiong, L. Ren, Pervaporation performance of quaternized poly(vinyl alcohol) and its crosslinked membranes for the dehydration of ethanol, *J. Membr. Sci.* 335 (1) (2009) 68–75.
- [20] J. Ge, Y. Cui, Y. Yan, W. Jiang, The effect of structure on pervaporation of chitosan membrane, *J. Membr. Sci.* 165 (1) (2000) 75–81.
- [21] Q. Li, Q. Liu, J. Zhao, Y. Hua, J. Sun, J. Duan, W. Jin, High efficient water/ethanol separation by a mixed matrix membrane incorporating MOF filler with high water adsorption capacity, *J. Membr. Sci.* 544 (2017) 68–78.
- [22] M. Nikbakht Fini, S. Soroush, M.M. Montazer-Rahmati, Synthesis and optimization of chitosan ceramic-supported membranes in pervaporation ethanol dehydration, *Membranes* 8 (4) (2018) 119.
- [23] Z. Xu, G. Liu, H. Ye, W. Jin, Z. Cui, Two-dimensional MXene incorporated chitosan mixed-matrix membranes for efficient solvent dehydration, *J. Membr. Sci.* 563 (2018) 625–632.
- [24] J. Yin, H. Tang, Z. Xu, N. Li, Enhanced mechanical strength and performance of sulfonated polysulfone/Tröger's base polymer blend ultrafiltration membrane, *J. Membr. Sci.* 625 (2021), 119138.
- [25] M.S. Abdul Wahab, S.A. Rahman, R.A. Samah, Hydrophilic enhancement of Polysulfone membrane via Graphene Oxide embedded thin film nanocomposite for Isopropanol dehydration, *Vacuum* 180 (2020), 109569.
- [26] C.-S. Hsu, R.M. Liou, S.-H. Chen, M.-Y. Hung, H.-A. Tsia, J.-Y. Lai, Pervaporation separation of a water-ethanol mixture by PSF-PEG membrane, *J. Appl. Polym. Sci.* 87 (13) (2003) 2158–2164.
- [27] S.-H. Chen, K.-C. Yu, S.-S. Lin, D.-J. Chang, R.M. Liou, Pervaporation separation of water/ethanol mixture by sulfonated polysulfone membrane, *J. Membr. Sci.* 183 (1) (2001) 29–36.
- [28] Y.M. Xu, T.-S. Chung, High-performance UiO-66/polyimide mixed matrix membranes for ethanol, isopropanol and n-butanol dehydration via pervaporation, *J. Membr. Sci.* 531 (2017) 16–26.
- [29] Y.M. Xu, S. Japip, T.-S. Chung, Mixed matrix membranes with nano-sized functional UiO-66-type MOFs embedded in 6FDA-HAB/DABA polyimide for dehydration of C1-C3 alcohols via pervaporation, *J. Membr. Sci.* 549 (2018) 217–226.
- [30] L.Y. Jiang, Y. Wang, T.-S. Chung, X.Y. Qiao, J.-Y. Lai, Polyimides membranes for pervaporation and biofuels separation, *Prog. Polym. Sci.* 34 (11) (2009) 1135–1160.
- [31] H. Yanagisita, C. Maejima, D. Kitamoto, T. Nakane, Preparation of asymmetric polyimide membrane for water/ethanol separation in pervaporation by the phase inversion process, *J. Membr. Sci.* 86 (3) (1994) 231–240.
- [32] Q.-F. An, M.B.M.Y. Ang, Y.-H. Huang, S.-H. Huang, Y.-H. Chiao, C.-L. Lai, H.-A. Tsai, W.-S. Hung, C.-C. Hu, Y.-P. Wu, K.-R. Lee, Microstructural characterization and evaluation of pervaporation performance of thin-film composite membranes fabricated through interfacial polymerization on hydrolyzed polyacrylonitrile substrate, *J. Membr. Sci.* 583 (2019) 31–39.
- [33] M.B.M.Y. Ang, S.-H. Huang, M.-W. Chang, C.-L. Lai, H.-A. Tsai, W.-S. Hung, C.-C. Hu, K.-R. Lee, Ultraviolet-initiated graft polymerization of acrylic acid onto thin-film polyamide surface for improved ethanol dehydration performance of pervaporation membranes, *Separ. Purif. Technol.* 235 (2020), 116155.
- [34] V. Freger, J. Gilron, S. Belfer, TFC polyamide membranes modified by grafting of hydrophilic polymers: an FT-IR/AFM/TEM study, *J. Membr. Sci.* 209 (1) (2002) 283–292.
- [35] J.A.D. Marquez, M.B.M.Y. Ang, B.T. Doma, S.-H. Huang, H.-A. Tsai, K.-R. Lee, J.-Y. Lai, Application of cosolvent-assisted interfacial polymerization technique to fabricate thin-film composite polyamide pervaporation membranes with PVDF hollow fiber as support, *J. Membr. Sci.* 564 (2018) 722–731.
- [36] D. Zheng, D. Hua, Y. Hong, A.-R. Ibrahim, A. Yao, J. Pan, G. Zhan, Functions of ionic liquids in preparing membranes for liquid separations: a review, *Membranes* 10 (12) (2020).
- [37] S. Tang, Z. Dong, X. Zhu, Q. Zhao, A poly(ionic liquid) complex membrane for pervaporation dehydration of acidic water-isopropanol mixtures, *J. Membr. Sci.* 576 (2019) 59–65.
- [38] X.-W. Liu, Y. Cao, Y.-X. Li, Z.-L. Xu, Z. Li, M. Wang, X.-H. Ma, High-performance polyamide/ceramic hollow fiber TFC membranes with TiO₂ interlayer for pervaporation dehydration of isopropanol solution, *J. Membr. Sci.* 576 (2019) 26–35.
- [39] H.-A. Tsai, Y.-L. Chen, S.-H. Huang, C.-C. Hu, W.-S. Hung, K.-R. Lee, J.-Y. Lai, Preparation of polyamide/polyacrylonitrile composite hollow fiber membrane by synchronous procedure of spinning and interfacial polymerization, *J. Membr. Sci.* 551 (2018) 261–272.
- [40] Y.-M. Wei, Z.-L. Xu, F.A. Qusay, K. Wu, Polyvinyl alcohol/polysulfone (PVA/PSF) hollow fiber composite membranes for pervaporation separation of ethanol/water solution, *J. Appl. Polym. Sci.* 98 (1) (2005) 247–254.
- [41] X. Zhang, M. Wang, C.-H. Ji, X.-R. Xu, X.-H. Ma, Z.-L. Xu, Multilayer assembled CS-PSS/ceramic hollow fiber membranes for pervaporation dehydration, *Separ. Purif. Technol.* 203 (2018) 84–92.
- [42] M. Thommes, K. Kaneko, A.V. Neimark, J.P. Olivier, F. Rodriguez-Reinoso, J. Rouquerol, K.S.W. Sing, Physisorption of gases, with special reference to the evaluation of surface area and pore size distribution (IUPAC Technical Report), *Pure Appl. Chem.* 87 (9–10) (2015) 1051–1069.
- [43] Y. Hasegawa, C. Abe, M. Nishioka, K. Sato, T. Nagase, T. Hanaoka, Formation of high flux CHA-type zeolite membranes and their application to the dehydration of alcohol solutions, *J. Membr. Sci.* 364 (1) (2010) 318–324.
- [44] I. Wenten, P. Dharmawijaya, P. Aryanti, R. Mukti, LTA zeolite membranes: current progress and challenges in pervaporation, *RSC Adv.* 7 (47) (2017) 29520–29539.
- [45] G. Gong, M. Mamoru, H. Nagasawa, M. Kanezashi, Y. Hu, T. Tsuru, Vapor-permeation dehydration of isopropanol using a flexible and thin organosilica membrane with high permeance, *J. Membr. Sci.* 588 (2019), 117226.
- [46] H. Guan, Y. Li, G. Gong, R. Xu, Y. Hu, T. Tsuru, Enhancing dehydration performance of isopropanol for flexible hybrid silica composite membranes with spray-coated active layer on polymers, *Separ. Purif. Technol.* 283 (2022), 120230.
- [47] N. Moriyama, Y. Kawano, Q. Wang, R. Inoue, M. Guo, M. Yokojii, H. Nagasawa, M. Kanezashi, T. Tsuru, Pervaporation via silicon-based membranes: correlation and prediction of performance in pervaporation and gas permeation, *AIChE J.* 67 (7) (2021), e17223.
- [48] N. Moriyama, H. Nagasawa, M. Kanezashi, T. Tsuru, Pervaporation dehydration of aqueous solutions of various types of molecules via organosilica membranes: effect of membrane pore sizes and molecular sizes, *Separ. Purif. Technol.* 207 (2018) 108–115.
- [49] S. Li, J. Dai, X. Geng, J. Li, P. Li, J. Lei, L. Wang, J. He, Highly selective sodium alginate mixed-matrix membrane incorporating multi-layered MXene for ethanol dehydration, *Separ. Purif. Technol.* 235 (2020), 116206.
- [50] S. Li, X. Geng, C. Ma, X. Zhan, J. Li, M. Ma, J. He, L. Wang, Improved performance of three-component structure mixed membrane for pervaporation modified by lignosulfonates@2D-MXene, *Separ. Purif. Technol.* 276 (2021), 119294.
- [51] T. Cao, J. Li, C. Li, N. Zhang, P. Cai, N. Wang, Q.-F. An, POSS-graphene oxide nanocomposite membranes for ethanol permselective pervaporation, *Microporous Mesoporous Mater.* 331 (2022), 111635.
- [52] X. Zhan, R. Ge, Z. Gao, T. Gao, L. Wang, J. Li, PVA-based MMMs for ethanol dehydration via pervaporation: a comparison study between graphene and graphene oxide, *Separations* 9 (2) (2022) 26.
- [53] Q. Wang, D. Astruc, State of the art and prospects in metal–organic framework (MOF)-Based and MOF-derived nanocatalysis, *Chem. Rev.* 120 (2) (2020) 1438–1511.
- [54] M. Liu, J. Wu, H. Hou, Metal–organic framework (MOF)-Based materials as heterogeneous catalysts for C–H bond activation, *Chem. Eur. J.* 25 (12) (2019) 2935–2948.
- [55] H. Konnerth, B.M. Matsagar, S.S. Chen, M.H.G. Prechtl, F.-K. Shieh, K.C.W. Wu, Metal–organic framework (MOF)-derived catalysts for fine chemical production, *Coord. Chem. Rev.* 416 (2020), 213319.
- [56] T.A. Goetjen, J. Liu, Y. Wu, J. Sui, X. Zhang, J.T. Hupp, O.K. Farha, Metal–organic framework (MOF) materials as polymerization catalysts: a review and recent advances, *ChemComm* 56 (72) (2020) 10409–10418.
- [57] C. Petit, Present and future of MOF research in the field of adsorption and molecular separation, *Curr. Opin. Chem. Eng.* 20 (2018) 132–142.
- [58] T. Ghanbari, F. Abnisa, W.M.A. Wan Daud, A review on production of metal organic frameworks (MOF) for CO₂ adsorption, *Sci. Total Environ.* 707 (2020), 135090.
- [59] C. Du, Z. Zhang, G. Yu, H. Wu, H. Chen, L. Zhou, Y. Zhang, Y. Su, S. Tan, L. Yang, J. Song, S. Wang, A review of metal organic framework (MOFs)-based materials for antibiotics removal via adsorption and photocatalysis, *Chemosphere* 272 (2021), 129501.
- [60] B.N. Bhadra, A. Vinu, C. Serre, S.H. Jhung, MOF-derived carbonaceous materials enriched with nitrogen: preparation and applications in adsorption and catalysis, *Mater. Today* 25 (2019) 88–111.
- [61] C.-K. Chang, H.J. Yu, H. Jang, T.-H. Hung, C.-K. Chang, J. Kim, J.S. Lee, D.-Y. Kang, Conformational-change-induced selectivity enhancement of CAU-10-PDC membrane for H₂/CH₄ and CO₂/CH₄ separation, *J. Membr. Sci. Lett.* 1 (1) (2021), 100005.
- [62] D.-S. Chiou, H.J. Yu, T.-H. Hung, Q. Lyu, C.-K. Chang, J.S. Lee, L.-C. Lin, D.-Y. Kang, Highly CO₂ selective metal–organic framework membranes with favorable coulombic effect, *Adv. Funct. Mater.* 31 (4) (2021), 2006924.
- [63] M.-Y. Kan, Q. Lyu, Y.-H. Chu, C.-C. Hsu, K.-L. Lu, L.-C. Lin, D.-Y. Kang, Suppressing defect formation in metal–organic framework membranes via plasma-assisted synthesis for gas separations, *ACS Appl. Mater. Interfaces* 13 (35) (2021) 41904–41915.
- [64] M.-Y. Kan, J.H. Shin, C.-T. Yang, C.-K. Chang, L.-W. Lee, B.-H. Chen, K.-L. Lu, J. S. Lee, L.-C. Lin, D.-Y. Kang, Activation-controlled structure deformation of pillared-bilayer metal–organic framework membranes for gas separations, *Chem. Mater.* 31 (18) (2019) 7666–7677.

- [65] X. Liu, C. Wang, B. Wang, K. Li, Novel organic-dehydration membranes prepared from zirconium metal-organic frameworks, *Adv. Funct. Mater.* 27 (3) (2017), 1604311.
- [66] K. Huang, Q. Li, G. Liu, J. Shen, K. Guan, W. Jin, A ZIF-71 hollow fiber membrane fabricated by contra-diffusion, *ACS Appl. Mater. Interfaces* 7 (30) (2015) 16157–16160.
- [67] H. Jin, K. Mo, F. Wen, Y. Li, Preparation and pervaporation performance of CAU-10-H MOF membranes, *J. Membr. Sci.* 577 (2019) 129–136.
- [68] L. Zhai, X. Yu, Y. Wang, J. Zhang, Y. Ying, Y. Cheng, S.B. Peh, G. Liu, X. Wang, Y. Cai, D. Zhao, Polycrystalline rare-earth metal-organic framework membranes with in-situ healing ability for efficient alcohol dehydration, *J. Membr. Sci.* 610 (2020), 118239.
- [69] Y.-J. Hsieh, C. Zou, J.-J. Chen, L.-C. Lin, D.-Y. Kang, Pillared-bilayer metal-organic framework membranes for dehydration of isopropanol, *Microporous Mesoporous Mater.* 326 (2021), 111344.
- [70] N. Hanikel, M.S. Prévot, F. Fathieh, E.A. Kapustin, H. Lyu, H. Wang, N.J. Diercks, T.G. Glover, O.M. Yaghi, Rapid cycling and exceptional yield in a metal-organic framework water harvester, *ACS Cent. Sci.* 5 (10) (2019) 1699–1706.
- [71] S. Cong, Y. Yuan, J. Wang, Z. Wang, F. Kapteijn, X. Liu, Highly water-permeable metal-organic framework MOF-303 membranes for desalination, *J. Am. Chem. Soc.* 143 (48) (2021) 20055–20058.
- [72] F. Fathieh, M.J. Kalmutzki, E.A. Kapustin, P.J. Waller, J. Yang, O.M. Yaghi, Practical water production from desert air, *Sci. Adv.* 4 (6) (2018), eaat3198.
- [73] D. Dubbeldam, S. Calero, D.E. Ellis, R.Q. Snurr, RASPA: molecular simulation software for adsorption and diffusion in flexible nanoporous materials, *Mol. Simulat.* 42 (2) (2016) 81–101.
- [74] W.L. Jorgensen, D.S. Maxwell, J. Tirado-Rives, Development and testing of the OPLS all-atom force field on conformational energetics and properties of organic liquids, *J. Am. Chem. Soc.* 118 (45) (1996) 11225–11236.
- [75] W.L. Jorgensen, J. Chandrasekhar, J.D. Madura, R.W. Impey, M.L. Klein, Comparison of simple potential functions for simulating liquid water, *J. Chem. Phys.* 79 (2) (1983) 926–935.
- [76] A.K. Rappe, C.J. Casewit, K.S. Colwell, W.A. Goddard, W.M. Skiff, UFF, a full periodic table force field for molecular mechanics and molecular dynamics simulations, *J. Am. Chem. Soc.* 114 (25) (1992) 10024–10035.
- [77] C. Zou, D.R. Penley, E.H. Cho, L.-C. Lin, Efficient and accurate charge assignments via a multilayer connectivity-based atom contribution (m-CBAC) approach, *J. Phys. Chem. C* 124 (21) (2020) 11428–11437.
- [78] A. Datar, M. Witman, L.-C. Lin, Improving computational assessment of porous materials for water adsorption applications via flat histogram methods, *J. Phys. Chem. C* 125 (7) (2021) 4253–4266.
- [79] A. Datar, M. Witman, L.-C. Lin, Monte Carlo simulations for water adsorption in porous materials: best practices and new insights, *AIChE J.* 67 (12) (2021), e17447.
- [80] A. Datar, M. Witman, L.-C. Lin, Responses to the Comments on “Monte Carlo Simulations for Water Adsorption in Porous Materials: Best Practices and New Insights”, *AIChE J.* n/a, 2022, e17684 n/a.
- [81] S. Plimpton, Fast parallel algorithms for short-range molecular dynamics, *J. Comput. Phys.* 117 (1) (1995) 1–19.
- [82] I.A. Lázaro, A comprehensive thermogravimetric analysis multifaceted method for the exact determination of the composition of multifunctional metal-organic framework materials, *Eur. J. Inorg. Chem.* 2020 (45) (2020) 4284–4294.
- [83] N. Hanikel, X. Pei, S. Chheda, H. Lyu, W. Jeong, J. Sauer, L. Gagliardi, O.M. Yaghi, Evolution of water structures in metal-organic frameworks for improved atmospheric water harvesting, *Science* 374 (6566) (2021) 454–459.
- [84] Y. Wang, Y. Ban, Z. Hu, Y. Zhao, M. Zheng, W. Yang, T. Zhang, Hetero-lattice intergrown and robust MOF membranes for polyol upgrading, *Angew. Chem. Int. Ed.* 61 (10) (2022), e202114479.
- [85] Y. Hu, X. Dong, J. Nan, W. Jin, X. Ren, N. Xu, Y.M. Lee, Metal-organic framework membranes fabricated via reactive seeding, *Chem. Commun.* 47 (2) (2011) 737–739.
- [86] S. Wang, Z. Kang, B. Xu, L. Fan, G. Li, L. Wen, X. Xin, Z. Xiao, J. Pang, X. Du, D. Sun, Wettability switchable metal-organic framework membranes for pervaporation of water/ethanol mixtures, *Inorg. Chem. Commun.* 82 (2017) 64–67.
- [87] Y. Hasegawa, H. Hotta, K. Sato, T. Nagase, F. Mizukami, Preparation of novel chabazite (CHA)-type zeolite layer on porous α -Al₂O₃ tube using template-free solution, *J. Membr. Sci.* 347 (1) (2010) 193–196.
- [88] A. Huang, W. Yang, J. Liu, Synthesis and pervaporation properties of NaA zeolite membranes prepared with vacuum-assisted method, *Separ. Purif. Technol.* 56 (2) (2007) 158–167.
- [89] H. Li, J. Xu, J. Wang, J. Yang, K. Bai, J. Lu, Y. Zhang, D. Yin, Seed-free synthesis of highly permeable zeolite NaA membranes through deposition of APTES-functionalized alumina particles on macroporous supports, *J. Membr. Sci.* 471 (2014) 84–93.
- [90] K. Sato, K. Sugimoto, N. Shimotsuma, T. Kikuchi, T. Kyotani, T. Kurata, Development of practically available up-scaled high-silica CHA-type zeolite membranes for industrial purpose in dehydration of N-methyl pyrrolidone solution, *J. Membr. Sci.* 409–410 (2012) 82–95.
- [91] T.-H. Hung, X. Deng, Q. Lyu, L.-C. Lin, D.-Y. Kang, Coulombic effect on permeation of CO₂ in metal-organic framework membranes, *J. Membr. Sci.* 639 (2021), 119742.